RMetS
Royal Meteorological Society

# Assimilation of water-vapour airborne lidar observations: impact study on the COPS precipitation forecasts

S. Bielli,[a] M. Grzeschik,[a] E. Richard,[a]* C. Flamant,[b] C. Champollion,[c] C. Kiemle,[d] M. Dorninger[e] and P. Brousseau[f]

[a]*Laboratoire d'Aérologie, CNRS and Université de Toulouse III, Toulouse, France*
[b]*Laboratoire Atmosphères, Milieux, Observations Spatiales, CNRS and Université de Paris VI, Paris, France*
[c]*Géosciences, CNRS and Université de Montpellier II, Montpellier, France*
[d]*Deutsches Zentrum für Luft- und Raumfahrt (DLR), Oberpfaffenhofen, Germany*
[e]*Department of Meteorology and Geophysics, University of Vienna, Vienna, Austria*
[f]*CNRM–GAME, Météo-France and CNRS, Toulouse, France*

*Correspondence to: E. Richard, Laboratoire d'Aérologie, 14 Avenue Belin, 31400 Toulouse, France.
E-mail: evelyne.richard@aero.obs-mip.fr

**The Convective and Orographically-driven Precipitation Study (COPS) carried out in summer 2007 over northeastern France and southwestern Germany provided a fairly comprehensive description of the low-troposphere water-vapour field, thanks in particular to the deployment of two airborne differential absorption lidar systems. These lidar observations were assimilated using the 3D-Var assimilation system of the Application of Research to Operations at MEsoscale (AROME) numerical weather prediction mesoscale model. The assimilation was carried out for the period 4 July–3 August by running a three-hour forward intermittent assimilation cycle. First, the impact of the lidar observations was assessed by comparing the analyses with a set of more than 200 independent soundings. The lidar observations were found to have a positive impact on the analyses by reducing the dry bias in the first 500 m above ground level and by diminishing the root-mean-square error by roughly 15% in the first km. Then the impact of the lidar observations was assessed by comparing the precipitation forecasts (obtained with and without the lidar observations for the period 15 July–2 August) with the gridded precipitation observations provided by the Vienna Enhanced Resolution Analysis. In general, the impact was found to be positive but not significant for the 24 h precipitation and positive and significant for the 6 h precipitation, with an improvement lasting up to 24 h. Some selected case studies show that the improvement was obtained through a better depiction of convection initiation or through a more accurate positioning of the precipitation systems.** Copyright © 2011 Royal Meteorological Society

*Key Words:* LEANDRE 2; WALES; AROME; VERA

*Received 2 February 2011; Revised 4 November 2011; Accepted 10 November 2011; Published online in Wiley Online Library 21 December 2011*

*Citation:* Bielli S, Grzeschik M, Richard E, Flamant C, Champollion C, Kiemle C, Dorninger M, Brousseau P. 2012. Assimilation of water-vapour airborne lidar observations: impact study on the COPS precipitation forecasts. *Q. J. R. Meteorol. Soc.* **138**: 1652–1667. DOI:10.1002/qj.1864

## 1. Introduction

Quantitative Precipitation Forecasts (QPFs) are of high socio-economic value and great efforts are constantly being made to improve their accuracy. In the last decade, a new generation of numerical weather prediction systems (NWPS) has been developed based upon non-hydrostatic formulations running at the convective scale,

including a fairly detailed representation of clouds and precipitation and able to assimilate mesoscale observations. In parallel, various field campaigns have been organized to collect the high-resolution datasets required for their validation, e.g. the Mesocale Alpine Programme (MAP: Bougeault *et al.*, 2001), the International H2O Project (IHOP: Weckwerth *et al.*, 2004), the Convective Storm Initiation Project (Browning *et al.*, 2007), the African Monsoon Multidisciplinary Analysis (Redelsperger *et al.*, 2006) and the recent Convective and Orographically-driven Precipitation Study (COPS). COPS took place in Summer 2007 over northeastern France and southwestern Germany and addressed the issue of convective precipitation in a region of moderate orography (Wulfmeyer *et al.*, 2008, 2011). The COPS field campaign was accompanied by an unprecedented modelling effort carried out in the framework of the MAP-D-PHASE project (Rotach *et al.*, 2009). More than 30 models of various resolutions (including more than a dozen high-resolution convection-permitting models) were run in real time during COPS.

Water vapour is a central element of the precipitation processes. It provides the raw material for hydrometeor formation and acts as a vector for the transport of latent heat. Its role is even more crucial for convective precipitation, which is strongly controlled by the availability of moisture present in the environment (Weckwerth *et al.*, 2004; Ducrocq *et al.*, 2002). However, accurate, high-resolution, three-dimensional moisture observations are not often available and the inaccuracy of synoptically analyzed fields, routinely used as initial moisture conditions for the models, is considered as a major source of QPF errors. During COPS, great effort was made to obtain fairly exhaustive documentation of the water-vapour field, which was sampled by several *in situ* and remote, ground-based and airborne instruments. In particular, two airborne water-vapour lidar systems provided unique information on the spatial distribution of the moisture field. The availability of this dataset offers a new opportunity to assess the impact of water-vapour assimilation in mesoscale NWPS.

Several recent studies have focused on the assimilation of moisture products derived from the Global Positioning System (Zus *et al.*, 2008; Boniface *et al.*, 2009; Yan *et al.*, 2009; Bauer *et al.*, 2011b), but so far very few attempts have been made to assimilate water-vapour lidar observations. The very first studies (Kamineni *et al.*, 2003, 2006) were based upon the three-dimensional variational (3D-Var) assimilation of the airborne Lidar Atmospheric Sensing Experiment observations in the Florida State University global NWPS. They revealed the beneficial impact of these data on the track and intensity forecasts of a few hurricanes. More recently, Wulfmeyer *et al.* (2006) have assimilated the IHOP airborne water-vapour lidar observations during an IHOP case study with the MM5 mesoscale NWPS and its four-dimensional variational (4D-Var) assimilation system. They concluded that for the analyzed case the forecast of convection initiation was improved. This work was further extended by Grzeschik *et al.* (2008) to assimilation of the observations provided by a ground-based network of Raman lidar systems. A very recent study on the assimilation of airborne lidar data collected in the western North Pacific into the European Centre for Medium-Range Weather Forecasts (ECMWF) global model found an overall small but positive influence of the additional humidity observations, and considerable forecast impact under certain conditions (Harnisch *et al.*, 2011). All these studies have shown encouraging results. However, they were based on a limited number of cases and did not allow general conclusions to be drawn in a statistical sense regarding the impact of water-vapour lidar observation assimilation on the QPF.

The present study makes use of a pre-operational version of the Météo-France Application of Research to Operations at MEsoscale (AROME) NWPS (Seity *et al.*, 2011) and its associated 3D-Var high-resolution assimilation system to evaluate the impact on the QPF of the COPS airborne lidar observations collected during July 2007. A continuous assimilation cycle updated every 3 h was run over a month to provide the initial conditions of a sequence of 30 h forecasts carried out over 19 consecutive days.

This article is organized as follows. Section 2 gives a short overview of the COPS field experiment. The AROME NWPS is presented in section 3. Section 4 describes the available water-vapour lidar observations. The impact of the lidar data assimilation is examined first for the water-vapour analyses (section 5) and then for the precipitation forecasts (section 6). Discussion and concluding remarks are provided in section 7.

## 2. COPS field experiment

The overarching goal of COPS was to advance the quality of forecasts of orographically induced convective precipitation by 4D observation and modelling of its life cycle (Wulfmeyer *et al.*, 2008, 2011). COPS took place from 1 June–31 August 2007 over northeastern France and southwestern Germany in a region of moderate orography including the Vosges, the Black Forest and the Swabian Jura. The observational strategy was based on the reinforcement of existing networks (e.g. radiosondes and GPS stations) and the deployment of various passive and active remote-sensing instruments (e.g. radiometers, radars, lidars) at five selected sites. In addition, several instrumented research aircraft conducted flight missions above (and occasionally upstream of) the COPS domain during specific periods of interest in July. Two of these aircraft were equipped with a water-vapour Differential Absorption Lidar (DIAL). The Lidar Embarqué pour l'étude de l'Atmosphère –Nuages, Dynamique, Rayonnement et cycle de l'Eau (LEANDRE 2) system (Bruneau *et al.*, 2001a) was operated from the Service des Avions Français Instrumentés pour la Recherche en Environnement (SAFIRE) Falcon and the WAter vapour Lidar Expriment in Space (WALES) system (Wirth *et al.*, 2009; Kiemle *et al.*, 2011) was installed on board the DLR Falcon. During COPS, a special focus was given to the intercomparison of the different lidar systems, and the relative bias between LEANDRE 2 and WALES was found to be less than 4% (Bhawar *et al.*, 2011) over the 0.5–4 km height range. More information on the COPS campaign can be found in Wulfmeyer *et al.* (2011) and references therein.

## 3. AROME numerical weather prediction system

All the analyses and forecasts were performed with the recently developed fine-scale AROME NWPS used in its quasi-operational version of 2008, designated as cycle 33. AROME is a non-hydrostatic model, based on an extension of the adiabatic equations of the Aire Limitée, Adaptation dynamique, Développement InterNational (ALADIN) limited-area NWPS (Bubnovà *et al.*, 1995; Bénard, 2004).

 

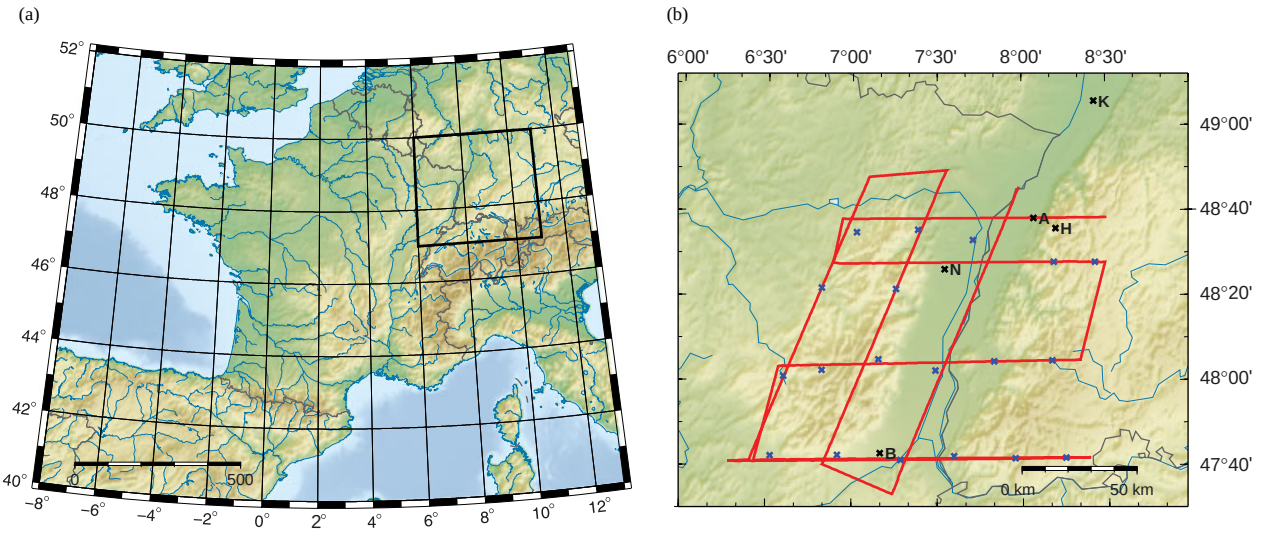


**Figure 1.** (a) AROME domain. The black square indicates the location of the COPS domain. (b) Topography of the COPS area and an example of a flight track corresponding to the SAFIRE Falcon flight performed on the morning of 26 July. The crosses indicate the position of the superobservation profiles included in the 0900 UTC analysis. The letters B, N, H, A, and K refer to the COPS additional soundings of Burnhaupt, Niederrott, Hornisgrinde, Achern, and Karlsruhe, respectively. This figure is available in colour online at wileyonlinelibrary.com/journal/qj

The AROME physical parametrizations are the same as those of the Meso-NH research model (Lafore *et al.*, 1998). They include a bulk microphysical scheme (Pinty and Jabouille, 1998) that governs the prognostic equations of six water species (vapour, cloud water, rainwater, primary ice, graupel and snow). No deep convection parametrization is used, as deep convection is assumed to be explicitly resolved. The turbulence scheme follows Cuxart *et al.* (2000) and the radiation is computed with the Rapid Radiative Transfer Model (Mlawer *et al.*, 1997). The surface energy exchanges are represented according to four possible surface-type patches (natural surfaces, urban areas, ocean, lake) included in a grid mesh. The Interactions Soil–Biosphere–Atmosphere scheme (ISBA: Noilhan and Mafhouf, 1996) is used for natural land surfaces, while energy exchanges over urban surfaces are parametrized according to the Town Energy Balance model (Masson, 2000). In this study AROME was run with a 2.5 km horizontal resolution over a domain centred over France and illustrated in Figure 1(a). It should be noted that the numerical set-up of the model differs substantially from the one used to produce the COPS real-time forecasts. The main differences are the location of the domain (centred over France instead of the Alps), an improved tuning of the numerical diffusion and the mesoscale assimilation, which was not yet implemented in July 2007.

The AROME data assimilation scheme (3D-Var/AROME) was derived from the 3D-Var/ALADIN system (Fischer *et al.*, 2005; Montmerle *et al.*, 2007) and is similar in terms of incremental formulation (Courtier *et al.*, 1994), observation operators, minimization method and data flow. Background-error covariances have been adapted to the higher resolution of AROME (Brousseau *et al.*, 2011a) and are estimated from an ensemble-based method (Berre *et al.*, 2006), built from a six-member ensemble of AROME forecasts carried out over two distinct 15 day periods. The two components of the horizontal wind, temperature, specific humidity and surface pressure are analyzed on the 2.5 km grid. The other model fields (e.g. microphysical variables) are provided from the AROME first-guess started from the previous analysis. The 3D-Var/AROME is run using a 3 h forward intermittent assimilation cycle. Each 3 h step computes an analysis using observations within a +/-1 h 30 assimilation window and a 3 h forecast to serve as first guess for the next step. More information regarding the assimilated observations can be found in Seity *et al.* (2011).

Three assimilation experiments were performed for a 30 day period extending from 4 July at 0000 UTC to 3 August at 0000 UTC. The control experiment (CTRL) was based on the standard observations and did not take any additional COPS observations into account. This choice was primarily made to stay as close as possible to the operational context. Moreover, it allowed the COPS observations to be used as independent data for validation purposes. The second experiment (LEAN) also considered the LEANDRE 2 water-vapour observations and the third experiment (LEWA) included both the LEANDRE 2 and WALES observations. From these three sets of AROME analyses, three 30 h AROME forecasts (F-CTRL, F-LEAN, and F-LEWA) were made starting at 0000 UTC and using the ALADIN operational forecasts as lateral boundary conditions.The forecast initial time was chosen as 0000 UTC and its duration was set at 30 h in order to optimize the precipitation verification, as most of the 24 h precipitation observations are collected between 0600 UTC and 0600 UTC on the following day. It is important to note that, due to the cycled assimilation, the three sets of forecasts differ not only in their initial fields but also in their first-guess fields (but they use the same boundary conditions). The forecast spanned the period from 15 July–2 August and corresponded to the time during which the aircraft were available.

## 4. Airborne lidar water-vapour observations

Most of the aircraft missions were carried out during the COPS Intensive Observation Periods (IOPs) that took place from mid-July to the beginning of August. The total water-vapour lidar dataset for this period corresponds to 22 hours of observations distributed over 10 days and 25 flights (12 for the SAFIRE Falcon and 13 for the DLR Falcon). Vertical profiles of water-vapour mixing ratio and water-vapour mixing ratio error below the flight level are available from

Table 1. Distribution of the available superobservation profiles with respect to the forecast period (15 July–2 August).

| Date | SAFIRE-FALCON flight type | Number of LEANDRE 2 superobservation profiles per analysis time (UTC) | | | | | | DLR-FALCON flight type | Number of WALES superobservation profiles per analysis time (UTC) | | | | | |
|---|---|---|---|---|---|---|---|---|---|---|---|---|---|---|
| | | 06 | 09 | 12 | 15 | 18 | 21 | | 06 | 09 | 12 | 15 | 18 | 21 |
| 07/14 | COPS | 00 | 04 | 22 | 00 | 00 | 00 | | | | | | | |
| 07/15 | COPS | 06 | 27 | 17 | 16 | 00 | 00 | COPS | 06 | 01 | 00 | 00 | 00 | 00 |
| 07/16 | COPS | 04 | 04 | 00 | 00 | 00 | 00 | | | | | | | |
| 07/17 | | | | | | | | | | | | | | |
| 07/18 | COPS | 00 | 00 | 04 | 11 | 00 | 00 | COPS | 00 | 00 | 00 | 20 | 01 | 00 |
| 07/19 | COPS | 00 | 00 | 10 | 22 | 00 | 00 | ETReC | 00 | 21 | 42 | 20 | 20 | 00 |
| 07/20 | COPS | 05 | 12 | 00 | 00 | 00 | 00 | COPS | 00 | 17 | 17 | 00 | 00 | 00 |
| 07/21 | | | | | | | | | | | | | | |
| 07/22 | | | | | | | | | | | | | | |
| 07/23 | | | | | | | | | | | | | | |
| 07/24 | | | | | | | | | | | | | | |
| 07/25 | COPS | 00 | 15 | 09 | 00 | 03 | 04 | COPS | 00 | 00 | 00 | 13 | 00 | 00 |
| 07/26 | COPS | 00 | 19 | 11 | 00 | 00 | 00 | COPS | 00 | 08 | 16 | 00 | 00 | 00 |
| 07/27 | | | | | | | | | | | | | | |
| 07/28 | | | | | | | | | | | | | | |
| 07/29 | | | | | | | | | | | | | | |
| 07/30 | | | | | | | | COPS | 00 | 00 | 12 | 00 | 00 | 00 |
| 07/31 | COPS | 00 | 00 | 00 | 00 | 04 | 03 | | | | | | | |
| 08/01 | COPS | 00 | 20 | 06 | 21 | 05 | 00 | ETReC | 40 | 46 | 20 | 29 | 20 | 00 |
| 08/02 | | | | | | | | | | | | | | |

the joint COPS/D-PHASE database, through the CERA interface of the World Data Centre for Climate (WCDD: http://cera-www.dkrz.de/CERA/). The original resolution of the lidar data was roughly 300 m in the vertical and 10 km in the horizontal. Table 1 gives a list of observation periods and the type of flight pattern performed for the two lidars. Most of the time, the two aircraft flew –in coordination whenever possible –over the COPS area along a mattress-like pattern, which was repeated for each IOP. This flight type is referred to as COPS. In addition the DLR Falcon performed a few upstream missions over France, Portugal and Spain, to collect largescale targeted observations upstream. This flight type, as it was performed in the context of THe Observing System Research and Predictability Experiment (THORPEX) European Regional Campaign (ETReC) is referred to as ETReC. Figure 1(b) shows the flight track (COPS type) of the SAFIRE Falcon on 26 July over the COPS area.

No specific operator was developed to assimilate the lidar observations, as the dropsonde operator could be used to handle the data. Nevertheless, before their assimilation into the 3D-Var assimilation system three main pre-processing steps were performed. First of all, an automatic procedure removed all unrealistic or suspicious data: all constant values at the bottom of each profile, which are artefacts from the ground surface, all negative errors and negative water-vapour values, absolute errors greater than 1.5 g kg$^{-1}$ and relative errors greater than 50% and smaller than 2% (to avoid giving the data too much weight). Then, additional manual exclusions were performed to remove remaining spurious values. Because of the high spatial resolution of the data, the second step consisted of upscaling the data to adapt them to the coarser resolution of the model. First, the water-vapour profiles were grouped into corresponding model analysis times within a 3 h window.Then each analysis group was scanned to find profiles within a 25 km range to perform the horizontal grouping. This distance of 25 km corresponds to the horizontal correlation length-scale of AROME background-error covariances for temperature and specific humidity (Brousseau *et al.*, 2011a). It represents the horizontal range of the background modification provided by an observation. To assimilate observations at a higher resolution is not useful and could become detrimental. Finally, a vertical grouping was performed within the range of thickness of the corresponding AROME levels. The mean values of each group were conflated to a new profile of superobservations with the mean position of the profile group. As for all kinds of observations, the lidar observation-error covariance matrix is diagonal, which means that only error variances were considered. The error of each superobservation was estimated as the square root of the sum of the squares of the observation standard deviation (to account for representativeness error) and the mean original error estimate (delivered by the data providers, see for instance Bruneau *et al.* (2001b) for its computation). As variational data assimilation needs both unbiased observations and an unbiased model, the third step, bias correction, consisted of correcting the data from eventual biases by comparing the observations with the analyses. In our case, each superobservation profile was compared with the 3 h forecast of the control experiment, in which all available observations except the LEANDRE 2 and WALES data were assimilated. The number of superobservation profiles included in each analysis is indicated in Table 1 and an example of their spatial distribution is given in Figure 1(b). Due to the averaging procedure, not all the superobservations are located on the aircraft track. In total, 653 (284 from LEANDRE 2 and 369 from WALES) superobservation profiles were assimilated.

## 5. Impact on the analyses

As a preliminary check, the results were examined using the standard verification tools, which are used operationally to monitor the AROME assimilation system. For each type of routine observations (e.g. synop, temp, satellite products), these tools compute the departure of the first guess and

 

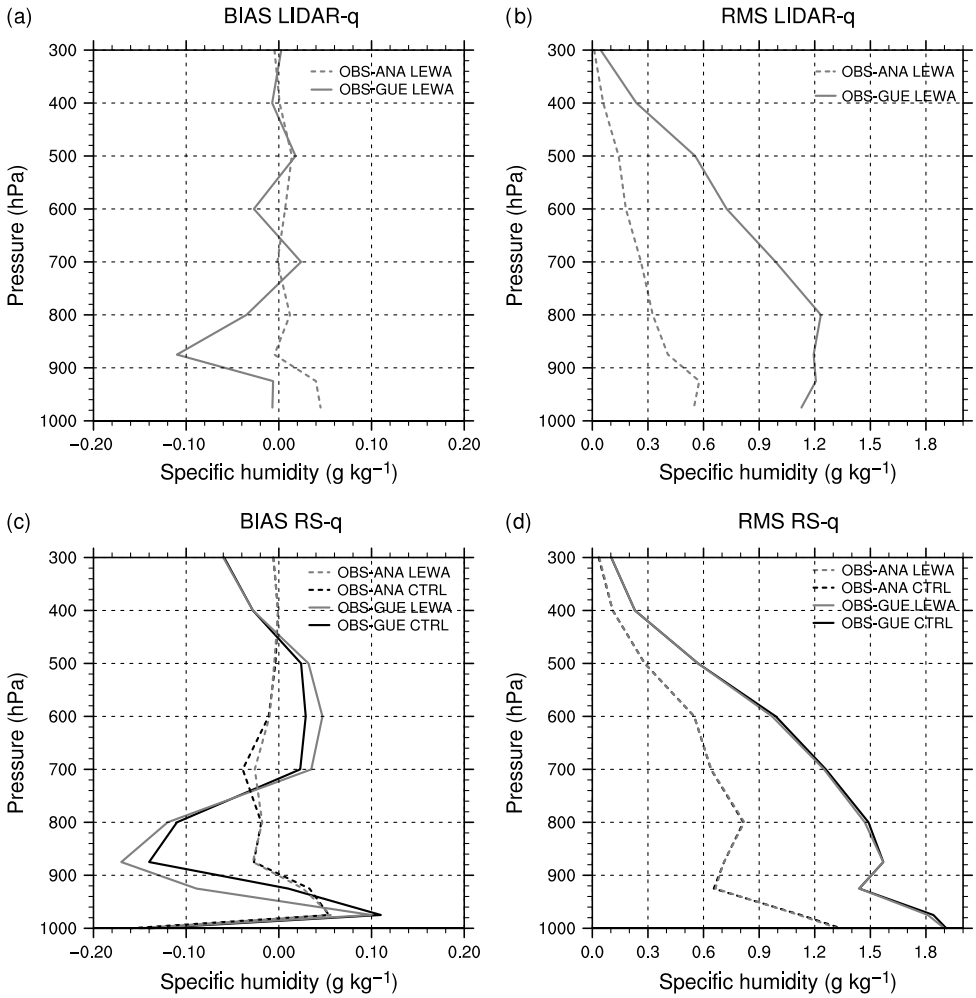


**Figure 2.** Comparison of first-guess and analysis departures with respect to (a) lidar and (c) operational radiosonde observations. Comparison of the first-guess and analysis RMSE with respect to (b) lidar and (d) operational radiosonde observations. Computation is made for the full AROME domain and for the period spanning 14 July–2 August.

analysis from the observations and also the associated root-mean-square errors (RMSEs). Figure 2 presents the results obtained for specific humidity from all lidar and temp observations included in the LEWA assimilation cycle. Figure 2 (a) and (b), corresponding to the lidar observations, shows that the lidar assimilation worked correctly. The bias and RMSE of the analysis departures from the observations are reduced compared with the values of the first-guess departures. Figure 2 (c) and (d), corresponding to the radiosonde observations, further indicates that the lidar assimilation did not induce large perturbations in the moisture field. Compared with CTRL, the bias of the first-guess departures from the observations increases but the bias of the analysis departures is very similar or marginally reduced (around the 700 hPa level), whereas the associated RMSEs remain nearly unchanged. These latter results were not unexpected, since most of the lidar observations were located in a very small portion of the AROME domain and should not impact the results too much over the whole AROME domain.

A more relevant assessment was obtained by comparing the analyses with the COPS additional radio soundings (RS). In total, 229 soundings from Karlsruhe, Burnhaupt, Niederrot, Achern and Hornisgrinde (see Figure 1(b) for the locations) were used. All these soundings, blacklisted in the three assimilation cycles, were independent data. They were used to compute the bias and RMSE of the three assimilation cycles over the whole period. Even though the additional COPS soundings provide the most frequent and accurate moisture observations available, they also might have errors (Agusti-Panareda *et al.*, 2009; Nuret *et al.*, 2008; Bock and Nuret, 2009). However, the different comparisons carried out during COPS between RS, dropsondes, ground-based and airborne lidar data did not reveal any suspicious bias in either the RS data or the lidar data. We therefore consider that the RS observations are a reliable reference. Figure 3(a) compares the bias of the three analyses. It reveals a significant reduction of the dry bias in the first 500 m above ground when lidar observations are included. Additional improvement is also noticeable in the 1–3 km layer, especially when the data of the two lidars are taken into account simultaneously. The improvement of the analysis is confirmed by the RMSE plot shown in Figure 3(b). In the 0–1 km layer, the RMSE is reduced by 15% when lidar data are assimilated, whichever lidar is considered. Figure 3(c) and (d) present the same comparison for the temperature. The cold bias in the boundary layer is slightly reduced in the first 500 m in both LEAN and LEWA, whereas the RMSE remains nearly unchanged. The temperature is sensitive to the assimilation of the lidar observations but to a lesser extent than the moisture. Winds (not shown) are only weakly affected. Therefore, it can be concluded that over the

 

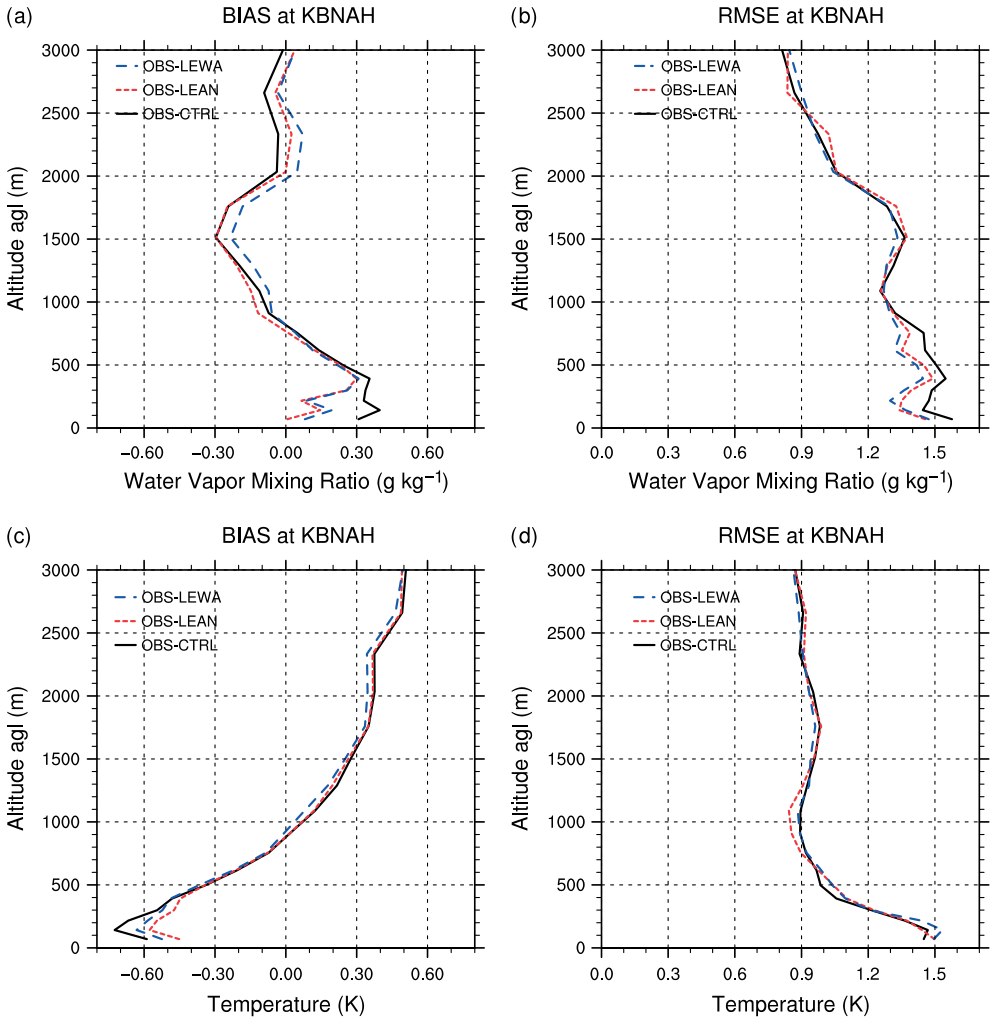


**Figure 3.** Biases and root-mean-square errors of the (a) and (b) water-vapour mixing ratio and (c) and (d) temperature obtained for the three analyses CTRL, LEAN and LEWA. The reference is provided by the additional COPS soundings performed at Karlsruhe, Burnhaupt, Niederrott, Achern and Hornisgrinde over the period spanning 14 July–2 August. This figure is available in colour online at wileyonlinelibrary.com/journal/qj

COPS domain the assimilation of the lidar observations has a large positive impact but this impact is mainly seen in the moisture analysis.

To illustrate the impact of lidar observations, we examine the case of July 15, which was characterized by isolated deep convection in the mid-afternoon over the Black Forest. This case was extensively studied during COPS (Barthlott *et al.*, 2011; Behrendt *et al.*, 2011; Richard *et al.*, 2011). Figure 4 shows the horizontal sections of the water-vapour mixing ratio at 2000 m at 0900 UTC and 1200 UTC for the CTRL and LEWA analyses and the superimposed lidar superobservations. Constrained by the lidar data, the horizontal water-vapour distribution is significantly modified. With respect to CTRL, LEWA appears drier over the Vosges and more humid over the northern Black Forest. It can also be noted that the modification extends further away than the observation area (see, for instance, the western and northern boundaries of the domain). It should be kept in mind that the analysis is sensitive not only to the observations included within the assimilation window considered in the current analysis but also to all the observations included in the previous ones.

Before assessing the impact of the lidar observations on the forecasts, it is worthwhile illustrating how the lidar observations (mostly obtained between 0600 UTC and 1800 UTC) propagate from one analysis to the next and how much lidar signal remains in the 0000 UTC analysis that is used to initialize the next forecast. Figure 5 presents the time evolution of the moisture increments (computed as the difference fields between LEAN and CTRL) at 3000 m for a sequence of consecutive analyses starting on 14 July at 0900 UTC (i.e. the time of the first lidar observations) and ending on 15 July at 0000 UTC (i.e. the initial time of the first forecast). At 0900 UTC, only nine superobservations profiles are available. They induce a drying effect, which concerns a large fraction of the COPS domain. Three hours later more observations are available. The moisture increment now has a tripole structure, which results from both the current observations and the memory of past observations. In consequence, the impact of the observations extends further to the northeast along the mean flow direction. Three hours later, no more observations enter the analysis but the impact of the previous observations is still well marked over the COPS area. It can be noted that some other discrepancies between the two analyses now start to grow far away from the COPS area (for instance in the vicinity of the Pyrenees). The latter increments are a consequence of the quality-check procedure. Due to very slight modifications in the analysis, the number of observations that are accepted or rejected is modified. This is especially true for the observations of

 

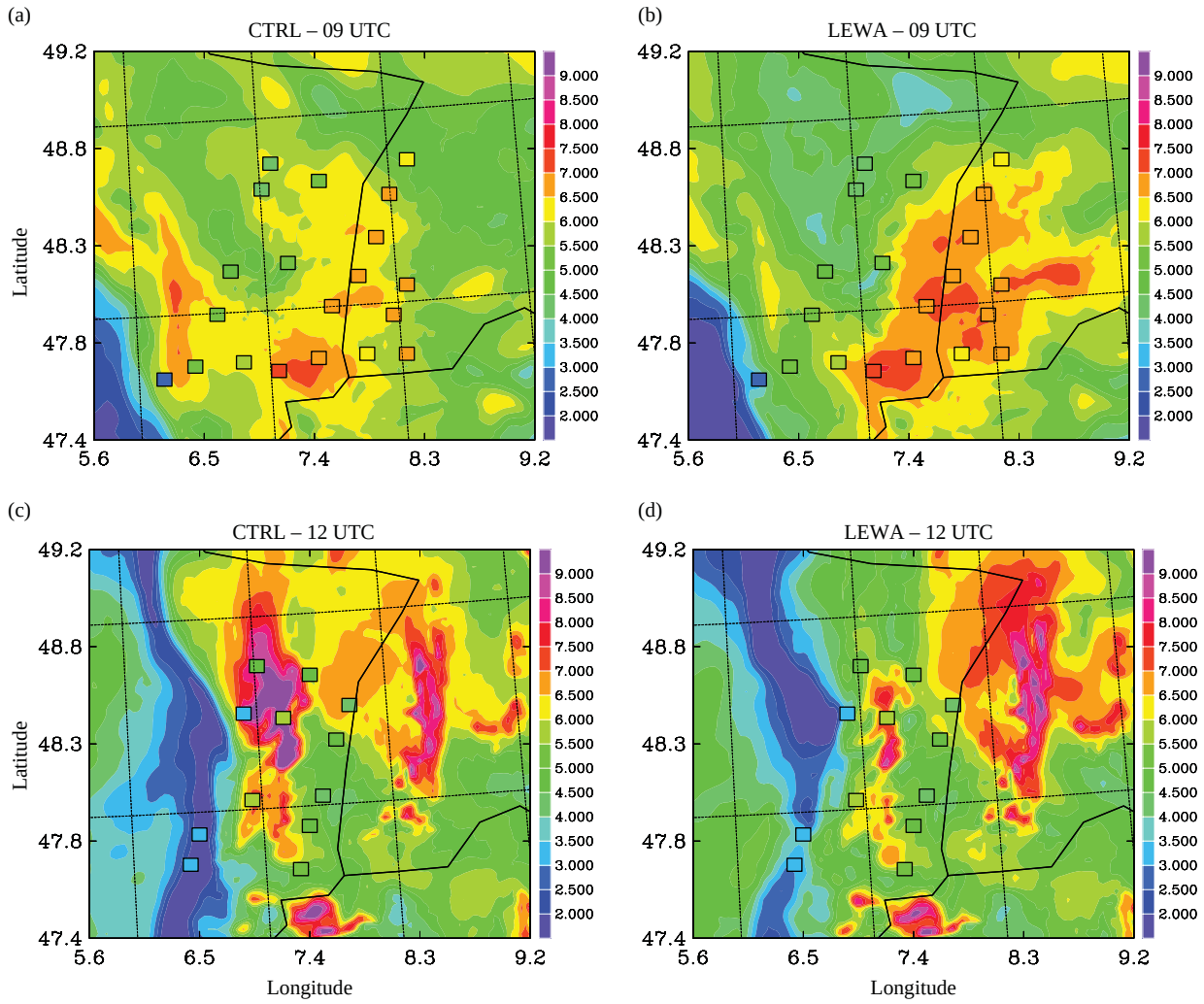


**Figure 4.** Analysis of the water-vapour mixing ratio (g kg$^{-1}$) at 2000 m on 15 July at 0900 and 1200 UTC for (a) and (c) CTRL and (b) and (d) LEWA, superimposed with the lidar superobservations (coloured squares).

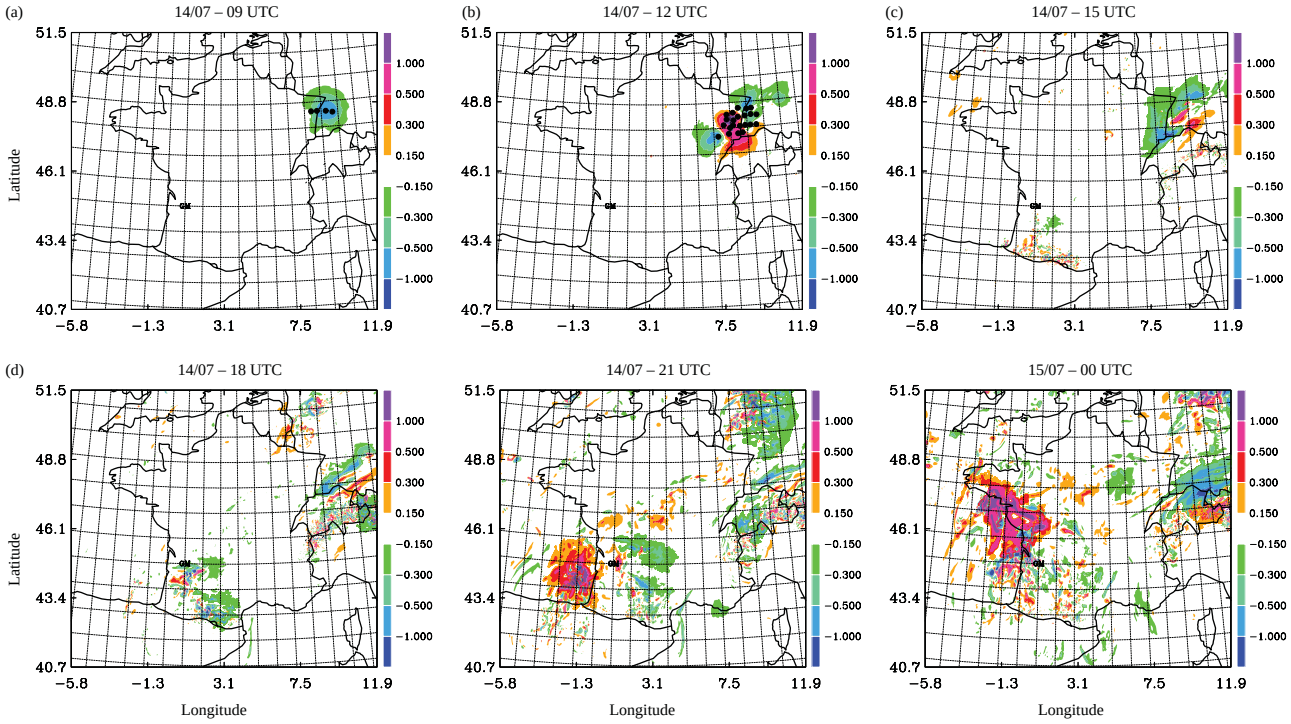


**Figure 5.** Time evolution of the water-vapour mixing ratio increments (in g kg$^{-1}$, computed as LEAN-CTRL) at 3000 m from 14 July at 0900 UTC to 15 July at 0000 UTC.

 

the surface stations located in mountainous areas. These increments grow with time and spread further in response to the convection that later develops over the Gulf of Biscay and propagates northwards. Meanwhile, the impact of the lidar observations over the COPS area is still discernible but becomes more and more diluted. These results tend to indicate that any eventual impact of the lidar observations on the 0000 UTC forecasts may result more from the continuous improvement of the analyses through the assimilation cycle than from the most recent observations, the direct effect of which is already quite diluted in the initial fields.

## 6. Impact on the precipitation forecasts

### 6.1. Methodology

Two different precipitation datasets were used to evaluate the impact of lidar data assimilation on the precipitation forecasts over the COPS domain. The first one (hereafter OBS) was based on the rain-gauge measurements. To maximize the number of observations, the accumulation period was selected to span the 24 hours from 0600 UTC to 0600 UTC on the following day. With this method, the number of available observations included in the COPS domain was of the order of 400 (as opposed to only 200 for an hourly accumulation period). The second dataset was provided by the Vienna Enhanced Resolution Analysis (VERA: Steinacker *et al.*, 2000, 2006; Dorninger *et al.*, 2008). VERA gridded accumulated precipitation analyses are available with an 8 km resolution and for different accumulation periods (1, 3, 6, 12 and 24 h). Approximately 1800 VERA grid points were included in the COPS domain. For each data set (OBS and VERA), the verification was made by considering the model field interpolated to the observation point. An alternative option consisting of averaging (and thus upscaling) the model fields on the VERA grid was found to have little impact on the results.

From the two datasets, standard verification methods were applied using continuous scores such as multiplicative bias (BIAS), mean absolute error (MAE), RMSE and correlation coefficient (COR) together with categorical scores such as false-alarm ratio (FAR), probability of detection (POD) and threat score (TS), calculated as a function of a varying precipitation threshold. All the formulae and further discussion of these scores can be found at http://www.cawcr.gov.au/projects/verification/. FAR, POD and TS vary in the range 0–1 and a good forecast is associated with high POD and TS and low FAR.

### 6.2. Whole period

A set of statistics was produced for the total precipitation over the whole period. This set was obtained for the observations by summing the 24 h precipitation measured between 0600 UTC and 0600 UTC on the following day and for the model by summing the 24 h precipitation within the 6–30 h forecast range of forecasts initialized at 0000 UTC. Table 2 shows the results of the continuous scores for the three experiments. In general, the AROME model was found to overpredict the precipitation, as indicated by bias values of the order of 1.1. This point has already been stressed by Bauer *et al.* (2011a), who analyzed the results of the COPS real-time forecasts. Assimilation of the lidar observations did not correct the overestimation. The bias was slightly reduced in F-LEAN and unchanged in F-LEWA. A more positive impact of the assimilation was obtained for the other scores. For both F-LEAN and F-LEWA, the mean absolute error was reduced by roughly 10% and the correlation coefficient increased by nearly 10%. It seems that the lidar observation assimilation had some positive impact on the precipitation forecast and that none of the forecasts with lidar assimilation clearly outperformed the others, but the significance of these results is not addressed.

Table 2. Comparison of the continuous scores obtained for the total precipitation sum computed over the COPS domain and for the whole forecast period.

| Experiment | BIAS | MAE (mm) | RMSE (mm) | COR (-) |
|---|---|---|---|---|
| F-CTRL | 1.09 | 24.3 | 31.6 | 0.54 |
| F-LEAN | 1.06 | 22.1 | 28.7 | 0.61 |
| F-LEWA | 1.09 | 22.5 | 31.3 | 0.59 |

Further, categorical scores were applied to the 24 h precipitation sums. The results are presented in Figure 6 in the form of score increments (with respect to the control forecast) and as a function of the precipitation threshold. Two sets of forecasts, F-LEAN and F-LEWA, were considered and the verification data were provided either by the OBS dataset or the VERA dataset. Whenever the impact of the assimilation is significant, all values in the confidence interval are on the same side of zero (either all positive or all negative). Starting with the OBS data set and the F-LEAN forecast, it seems that the precipitation forecasts are slightly improved for precipitation thresholds in the range 13–19 mm. In that range, the false-alarm ratio decreases whereas the probability of detection and the threat score increase. However, this improvement is not significant. In F-LEWA, the positive impact is more pronounced and also occurs over a more extended range of precipitation thresholds (8–25 mm), but it can also be observed that F-LEWA performs slightly worse than F-LEAN for low precipitation thresholds (0–3 mm). These results remain insignificant. The results using the VERA dataset show the same trends, with improvements for thresholds exceeding 5 mm for both forecasts and degradations for low thresholds in F-LEWA. However, due to a larger number of verification points the confidence interval is narrower and some results now appear to be significant, mainly in the range 10–20 mm and mainly for F-LEAN.

Additional statistics were produced for shorter precipitation accumulation periods. The most striking results were obtained by considering the six-hourly accumulated precipitation. Figure 7 shows the score increments obtained for the different 6 h periods of the forecasts and using the VERA dataset for verification. In the first 6 h (0000–0600 UTC) the precipitation forecast is clearly, and this time significantly, improved. This is true for both F-LEAN and F-LEWA, but F-LEWA appears to give better results in the sense that the results are significant over a wider range of precipitation threshold. For the next 6 h (0600–1200 UTC), the results are no more significant for F-LEAN but exhibit a substantial improvement for F-LEWA. During the afternoon (1200–1800 UTC), for both forecasts the results are

 

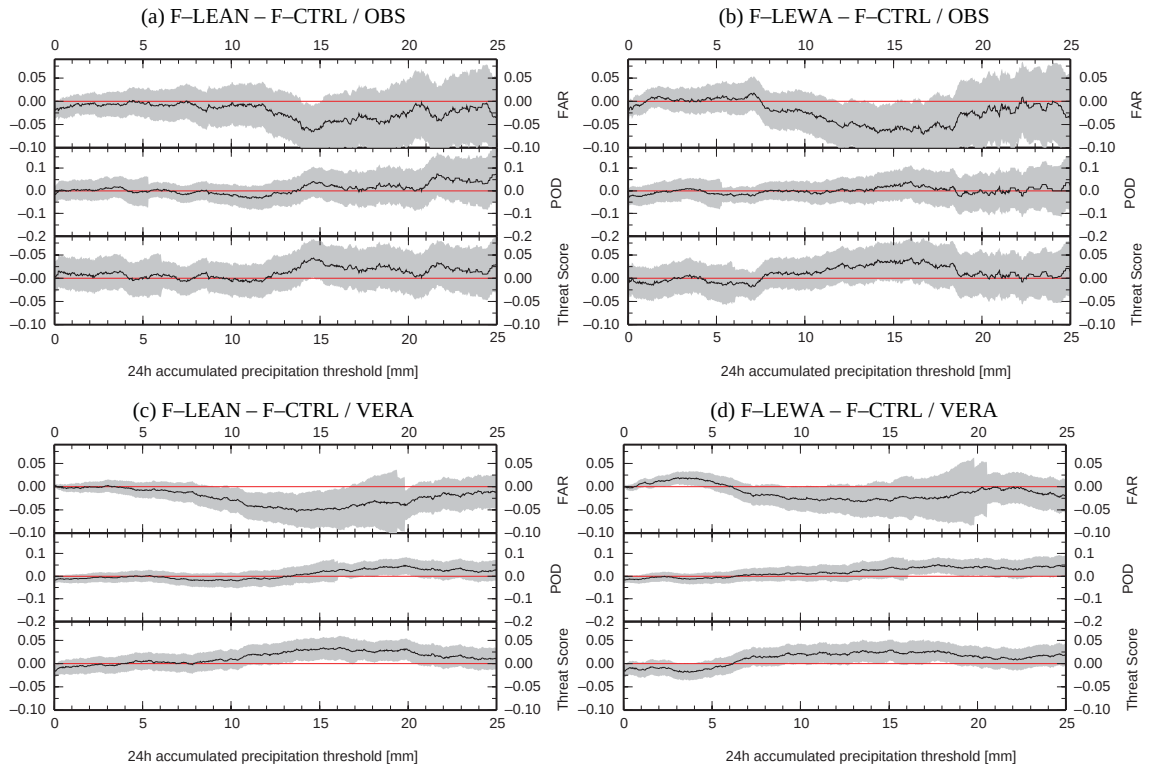


**Figure 6.** Score differences computed over the COPS domain for the 24 h precipitation accumulated from 0600 UTC to 0600 UTC on the following day and for the whole forecast period. In (a) and (b) the reference is provided by rain-gauge observations and in (c) and (d) by the VERA precipitation analysis. The shading represents the 95% confidence interval. This figure is available in colour online at wileyonlinelibrary.com/journal/qj

no longer significant or even slightly negative. Improvement is found again for the 1800–2400 UTC forecast range, not for the POD but for the FAR and TS, which are improved by nearly 0.1 up to the 15 mm threshold. For the last period (0000–0600 UTC on the following day, not shown) no significant results were obtained. In conclusion, the assimilation of the water-vapour lidar data is found to have a rather positive impact on the 6 h precipitation forecast and this impact is discernible up to 24 h of forecast. However, and contrary to expectations, this positive impact is not achieved for the afternoon period. Two reasons may explain the different behaviours obtained between the afternoon and early night periods. Firstly, over the COPS domain, the afternoon precipitation forecasts are particularly poor and remain poor whatever analysis is used. During this period, the correlation coefficient is very low for all the experiments, less than 0.2, whereas it exceeds 0.5 for the other periods and the bias is notably higher than for the other periods. Since the forecast is too far from reality, the assimilation does not help to improve the forecast. Secondly, July 2007 was abnormally moist and during the forecast period the COPS area was crossed by a sequence of frontal and mesoscale convective system passages (Bauer *et al.*, 2011a). As a result, the daily precipitation cycle did not show the usual summertime mid-afternoon peak but instead an early night maximum, not especially connected with the diurnal heating forcing but rather with the timing of the synoptic perturbations. This more intense precipitation, usually associated with organized systems, was in general better forecast and more likely to be improved by the assimilation of additional observations. In contrast, the patchier patterns of afternoon precipitation were more difficult to forecast accurately. Furthermore, the double-penalty issue associated with classical categorical scores was probably more acute for these fields and may have prevented a fair assessment of the results.

In general, F-LEWA was found to provide better results than F-LEAN. It can be hypothesized that the impact of the observations collected upstream during the ETReC flights was advected and felt later and thus longer over the COPS area. However, the analysis of the day-by-day results did not show a clear connection between the forecast improvement and the presence of an ETReC flight at a time close to the initial analysis. It is likely that the better performance of F-LEWA observations should be ascribed to a more complete description of the moisture field over the COPS area due to the larger number of lidar observations rather than to a better description of the upstream environment.

### 6.3. *Selected cases*

Using the same methodology, the 24 h precipitation scores were produced for each of the 19 days of the forecast period. In most cases the impact of the assimilation was found to be positive but not always significant. However, a clearer signal was obtained for a few cases, which are discussed in more detail below.

#### 6.3.1. *Case of 19 July*

Among the 19 days of the forecast period, the case of 19 July was the one for which the positive impact of the assimilation was largest. On that day, the COPS domain was affected by the remnants of a mesoscale convective system (MCS) that had developed over central France and moved

 

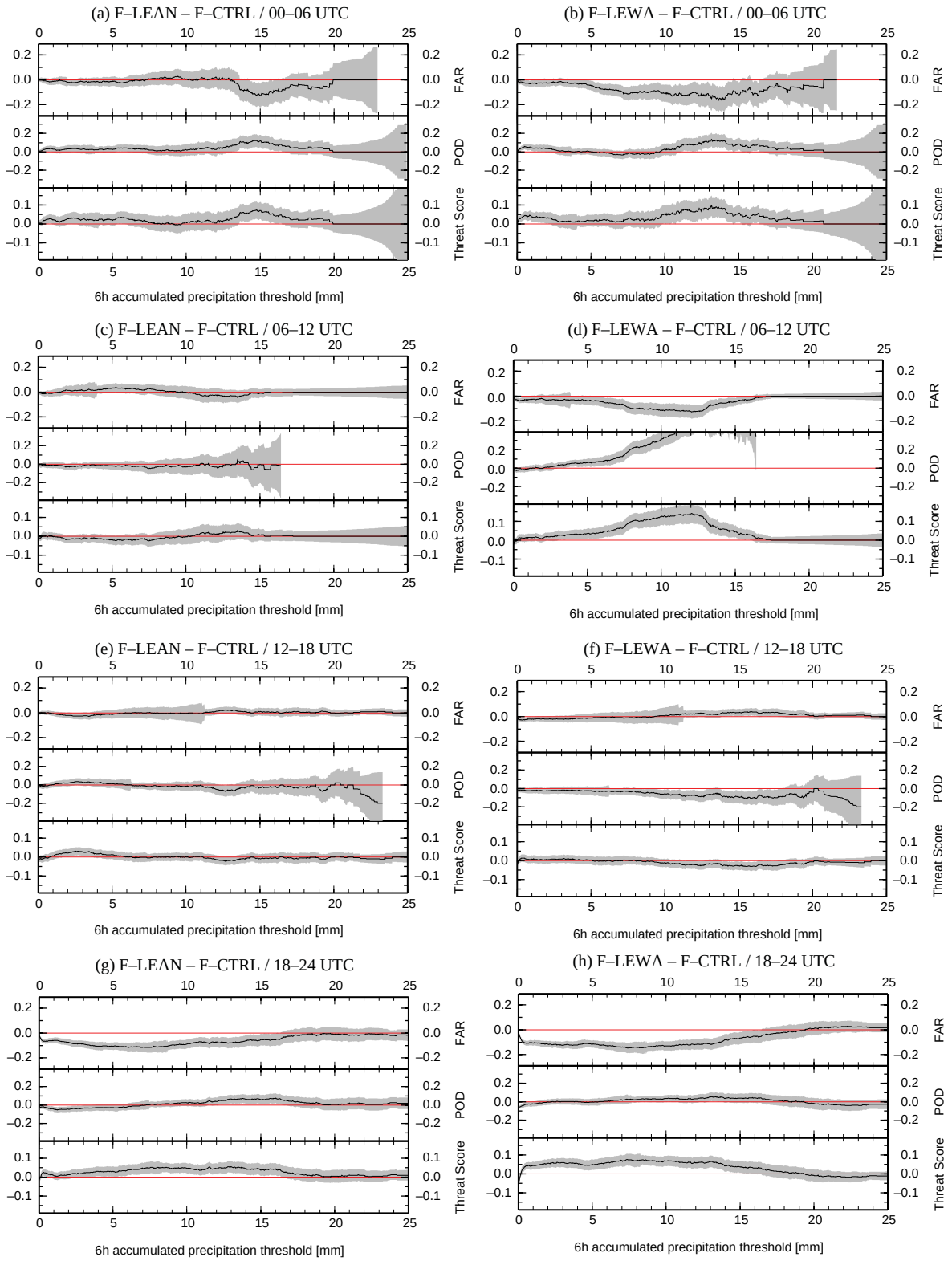


**Figure 7.** Score differences between F-LEAN and F-CTRL (left) and between F-LEWA and F-CTRL (right) computed over the COPS domain for 6 h precipitation for (a) and (b) 0000–0600 UTC, (c) and (d) 0600–1200 UTC, (e) and (f) 1200–1800 UTC and (g) and (h) 1800–2400 UTC. The reference is provided by the VERA precipitation analysis. The shading represents the 95% confidence interval. This figure is available in colour online at wileyonlinelibrary.com/journal/qj

to the northeast. Scores for the 6 h to 30 h forecast range (Figure 8(a) and (b)) reveal a significant improvement for both forecasts and also a better performance of F-LEWA compared with F-LEAN. In F-LEWA, the threat score is improved by up to 0.1 and the POD by up to 0.2 for a large range of precipitation thresholds. The corresponding precipitation fields are shown in Figure 9, together with the VERA analyzed field. The different forecasts do not match the VERA analysis well and all three experiments overpredict the 24 h accumulated precipitation. As already noted, this was a general trend of the model but on this day the relative bias was of the order of 2, compared with 1.1 on average

 

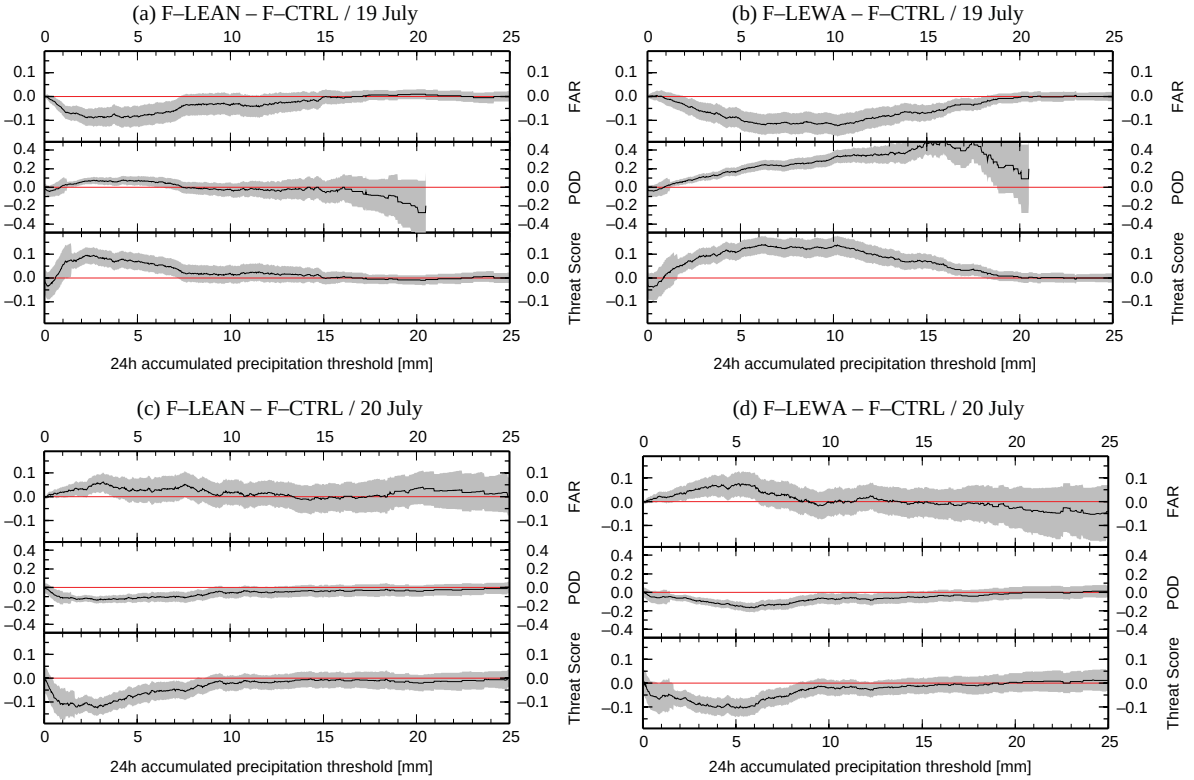


**Figure 8.** Score differences computed over the COPS domain for the 24 h precipitation accumulated from (a) and (b) 19 July 0600 UTC–20 July 0600 UTC and from (c) and (d) 20 July 0600 UTC–21 July 0600 UTC. The reference is provided by the VERA precipitation analysis. The shading represents the 95% confidence interval. This figure is available in colour online at wileyonlinelibrary.com/journal/qj

for the whole forecast period. Despite this overprediction, the impact of the assimilation appears clearly. In the case of F-LEAN, the precipitation is reduced on the eastern side of the domain, whereas in the case of F-LEWA the southwest–northeast oriented precipitation band is better located. This band, which is associated with the former MCS, crossed the COPS domain in the morning, whereas the more scattered structures seen in the south correspond to convective cells that developed over Switzerland in the afternoon. In all three forecasts these smaller-scale structures are not well captured.

This case matches our expectations in the sense that the forecast is improved by the assimilation of the LEANDRE 2 observations and further improved by additionally assimilating the WALES observations. However, the link with the observations is not straightforward, as both forecasts are improved but are improved in different ways. For instance, the benefit of LEANDRE observations leading to the reduction of precipitation over the eastern part of the domain does not persist when LEANDRE and WALES are assimilated simultaneously. Very similar results were obtained for the case of 17 July (not shown), presenting a similar banded precipitation pattern. More generally, the cases that are improved by the assimilation of the lidar observations are associated with organized (as opposed to scattered) precipitation patterns.

### 6.3.2. *Case of 20 July*

Over the whole period, a significant degradation of the forecasts was only observed for the case of 20 July. On the previous day, an ETReC mission over France and Portugal was performed and targeted observations were collected in sensitive areas by the German Falcon. However, the precipitation scores computed for the 6 h to 30 h forecast range (Figure 8(c) and (d)) reveal a significant degradation of both forecasts for precipitation thresholds below 10 mm. The corresponding precipitation fields are shown in Figure 10. On 20 July, the precipitation over the COPS area resulted from a complex interaction between the southern tip of a decaying MCS, which had developed over central Burgundy in France and propagated northeastwards, and changing terrain features. When the system crossed the COPS area (at around 1000 UTC), it became less active, particularly over the Rhine valley. Later on, it gained strength again and took on a bow-like structure. In the observed precipitation field (Figure 10(a)), the northwestern maximum occurs in the morning whereas the southern and eastern maxima occur in the late afternoon and correspond to the southern tip of the bow. The precipitation pattern is made even more complex by the convection intensification over the orography (Kottmeier *et al.*, 2008), which is particularly clear over the Vosges. The control experiment F-CTRL reproduced some, but not all, of these features. In particular, the eastern maximum was not captured by the model. F-LEAN and F-LEWA presented roughly the same weaknesses as F-CTRL. However, they provided a less accurate description of the northwestern precipitation core and also weaker precipitation over the Rhine valley.

Owing to their low predictability, clearly seen in the ensemble ECMWF forecasts, the cases of 20 July and 2 August were selected for ETReC missions with the expectation that targeted observations performed on the previous day would improve the forecast. However, for these two cases, the assimilation experiments were not successful and had a

 

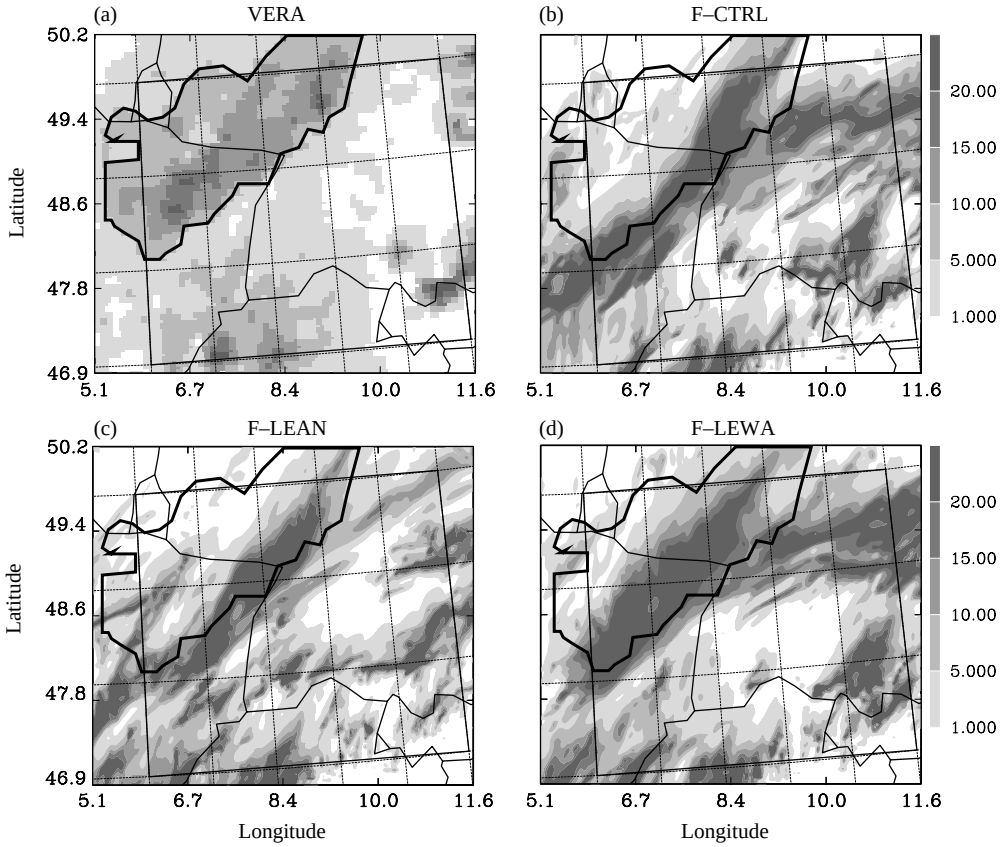


**Figure 9.** 24 h accumulated precipitation (mm) from 19 July 0600 UTC–20 July 0600 UTC: (a) VERA analysis, (b) F-CTRL, (c) F-LEAN and (d) F-LEWA. The thick black contour recalls the 5 mm contour of the observed main precipitation core.

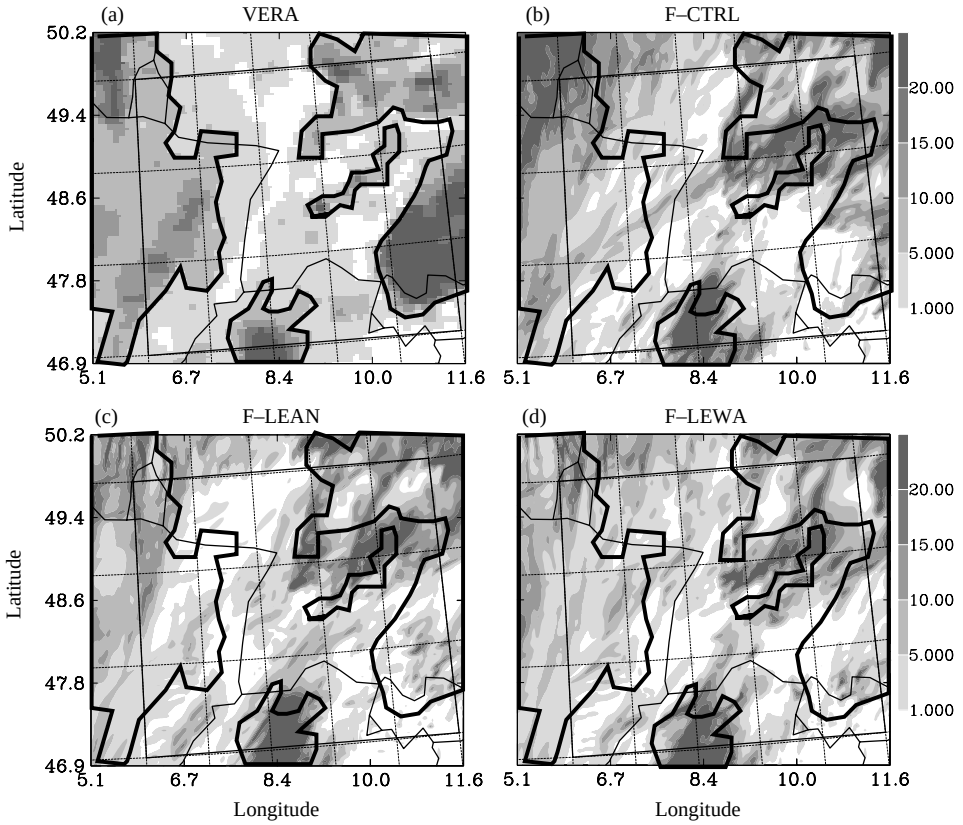


**Figure 10.** Same as 9 but from 20 July 0600 UTC–21 July 0600 UTC.

 

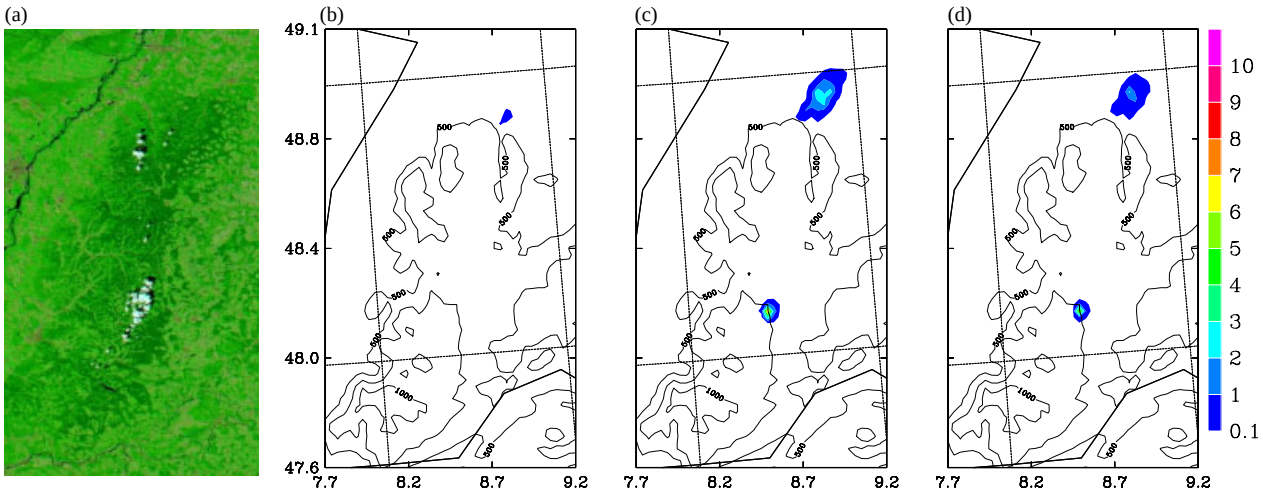


**Figure 11.** Enlargement over the Black Forest on 15 July: (a) RGB image of bands 7, 2, 1 of the MODIS instrument on the AQUA satellite, horizontal resolution 250 m, 1215 UTC picture, and forecast accumulated precipitation between 1200 and 1800 UTC from (b) F-CTRL, (c) F-LEAN and (d) F-LEWA. This figure is available in colour online at wileyonlinelibrary.com/journal/qj

negative impact (as shown above for 20 July) or a neutral impact (2 August, not shown) on the precipitation forecast. Various reasons could explain this lack of success. Firstly, the AROME domain considered in our study was not large enough to take advantage of all the available observations and most of the observations collected over southern Spain and Portugal (which were probably the most valuable ones in terms of sensitivity) did not enter the assimilation system. Secondly, the assimilation of only the water-vapour observations, only coupled to the dynamics through the background-error cross-correlations, might not have been sufficient to obtain the expected improvement.

#### 6.3.3. *Case of 15 July*

During COPS, only few cases of pure air-mass convection were observed. Among these, the case of 15 July stood out as a 'golden day' of the campaign, as convection occurred unexpectedly in a marginally unstable environment (Kalthoff *et al.*, 2009) and most of the D-PHASE models were unable to capture the event (Barthlott *et al.*, 2011). In the early afternoon a line of convective clouds reaching up to a height of 12 km developed over the Black Forest, as shown in Figure 11(a), corresponding to the early development phase. Radar observations (not shown) indicated that mainly the southern part of the cloud system was associated with deep convection and significant precipitation (see Behrendt *et al.*, 2011 or Richard *et al.*, 2011 for a more detailed description). Figure 11(b)–(d) shows the 6 h accumulated precipitation (from 1200–1800 UTC) for the three additional forecasts F-CTRL, F-LEAN and F-LEWA initialized at 1200 UTC (instead of 0000 UTC). F-CTRL produces very weak precipitation at the northern tip of the Black Forest but completely fails to capture the main storm, whereas F-LEWA and especially F-LEAN are quite successful in reproducing this storm and in particular its precise location. This result is consistent with the fact that the assimilation of the lidar observations significantly increases the moisture over the Black Forest, as was shown in Figure 4.

However, these satisfactory results were only obtained for the forecasts initialized at 1200 UTC (none of the 0000 UTC forecasts produced convection). We therefore cannot exclude that the analysis carried out over the whole period might have led to better results for a set of forecasts initialized at 1200, 1500 or 1800 UTC, which would have taken better and more direct advantage of the lidar observations.

## 7. Conclusion

The COPS field experiment carried out in summer 2007 over northeastern France and southwestern Germany provided a fairly good description of the spatial structure and time evolution of the low-troposphere water-vapour field, thanks to the deployment of two airborne DIAL lidar systems, LEANDRE 2 and WALES. Most of the available data were collected over the COPS area. Supplementary to this, a set of additional WALES observations was collected upstream in the framework of ETReC.

Water-vapour lidar observations were included in the 3D-Var assimilation system of the AROME numerical weather prediction model. The assimilation was carried out for the period of 4 July–3 August by running a continuous sequence of 3 h forward intermittent cycles. Three assimilation experiments were performed: a control experiment based on the only routine observations and two additional experiments in which the lidar observations of LEANDRE 2 and of LEANDRE 2 and WALES together were included.

The impact of the lidar observation assimilation on the analyses was addressed by comparing the three water-vapour analyses with the independent information provided by the additional COPS radio soundings, blacklisted in the analyses. The lidar observations were found to have a positive impact on the analyses by reducing the moist bias in the first 500 m above ground level and also by diminishing the root-mean-square error by roughly 15% in the first km. When both lidar systems were used simultaneously, bias improvement was also obtained at higher altitudes, up to 3 km.

Three sets of 30 h forecasts starting at 0000 UTC were performed from the three analyses for the period 15 July–2 August. The impact of the lidar observation assimilation on the precipitation forecast was first assessed by comparing the observed and forecast precipitation sum. The lidar observation assimilation yielded a 10% reduction of the

 

mean absolute errors and a 10% increase in the correlation coefficient.

Categorical scores for the daily precipitation sums were computed from 0600 UTC to 0600 UTC on the following day over the whole forecast period and using either the rain-gauge observations or the VERA precipitation analysis for reference. The forecasts based on the assimilation of the lidar observations showed signs of improvement, with a decrease in the false-alarm ratio and an increase in the probability of detection and threat score for a wide range of precipitation thresholds. However, this improvement was found to be non-significant with respect to the 95% confidence level (when the reference was provided by the observations) or only marginally significant (when the reference was based on the VERA analysis), which indicates a limited impact of the lidar assimilation on the 24 h precipitation forecast.

The same methodology was applied to the six-hourly precipitation forecasts, using the VERA analysis. In general, these results revealed a positive and significant impact of the lidar observations, discernible for up to 24 h. However, this conclusion did not hold for the afternoon period, for which the three forecasts provided equal and particularly poor results. The forecasts assimilating both sets of lidar systems appear to perform slightly better than the forecast using only LEANDRE 2 observations.

To gain further insight into these results, a few case studies were analyzed in more detail. The case of 19 July, for which the strongest positive impact was obtained, showed that the major source of improvement was a better positioning of the precipitation band that swept the COPS domain. In contrast, in the case of 20 July, associated with a complex and scattered precipitation pattern, the three forecasts exhibited poor skill and the assimilation of the lidar observations was even found to be detrimental. As opposed to these two cases associated with strong embedded convection, the case of 15 July was a very good example of pure air-mass convection, for which observations representative of the mesoscale are expected to have a strong imppact. Whereas the control forecast was not able to capture the isolated storm that developed over the southern Black Forest, the two experiments in which the lidar observations were assimilated showed better results and were able to capture the location and timing of convection initiation.

These results are encouraging, although they deserve further investigation. Future work will be carried out with a more recent version of the AROME numerical weather prediction system, which has undergone many improvements since 2007, as much in the model itself as in the assimilation procedure. In particular, better background-error statistics, for instance based on flow-dependent background-error covariances (which tend to increase the coupling between temperature and moisture errors in the case of convection: Brousseau *et al.*, 2011b), could bring significant improvement. The assimilation of the COPS observations will also be extended to the water-vapour observations of the ground-based lidars and to the wind observations of the DLR Doppler wind lidar, which flew on the same platform as the WALES system. In the longer term, it would desirable to extend this work to other data-assimilation systems such as ensemble Kalman filters, which may be more optimal or at least easier to operate than a variational system.

**Acknowledgements**

The support of the World Weather Research Program (WWRP) in the scientific planning of COPS and excellent collaboration with the D-PHASE modelling community were greatly appreciated. COPS is a component of Priority Program 1167 funded by the German Research Foundation. COPS was further supported by Institut des Sciences de lÚnivers (CNRS/INSU), Centre National de la Recherche Spatiale (CNES), Agence Nationale pour la Recherche (ANR) and Météo-France, and also by the Austrian Science Foundation (FWF) and the University of Vienna. The authors thank the Service des Avions Français Instrumentés pour la Recherche en Environnement (SAFIRE: www.safire.fr), the Institut Géographique National (IGN: www.ign.fr) and the Division Technique of INSU (DT/INSU: www.dt.insu.cnrs.fr) for preparing and delivering the research aircraft (Falcon 20/F-GBTM) and the airborne instruments in a timely manner for COPS. The authors are grateful to D. Bruneau and P. Genau (LATMOS), F. Blouzon, A. Abchiche and N. Amarouche (DT/INSU) for refitting and operating the LEANDRE 2 system in the F/F20 and to G. Jaubert and M. Nuret for their assistance with the assimilation system. Computational resources were provided by Météo-France and Grand Equipement National de Calcul Intensif (GENCI, project 100569-CP1).

**References**

Agusti-Panareda A, Vasiljevic D, Beljaars A and Bock O, Guichard F, Nuret M, Garcia Mendez A, Ansersson E, Bechthold P, Fink A, Hersbach H, Lafore JP, Ngamini JB, Parker D, Redelsperger JL, Tompkins A. 2009. Radiosonde humidity bias correction over the West African region for the special AMMA reanalysis at ECMWF. *Q. J. R. Meteorol. Soc.* **135**: 595–617.

Barthlott C, Burton R, Kirshbaum D, Hanley K, Richard E, Chaboureau JP, Trentmann J, Kern B, Bauer HS, Schwitalla T, Keil C, Seity Y, Gadian A, Blyth A, Mobbs S, Flamant C, Handwerker J. 2011. Initiation of deep convection at marginal instability in an ensemble of mesoscale models: A case study from COPS. *Q. J. R. Meteorol. Soc.* **137**: 118–136.

Bauer HS, Weusthoff T, Dorninger M, Wulfmeyer V, Schwitalla T, Gorgas T, Arpagaus M, Warrach-Sagi K. 2011a.. Predictive skill of a subset of models that participated during D-PHASE in the COPS region. *Q. J. R. Meteorol. Soc.* **137**: 287–305.

Bauer HS, Wulfmeyer V, Schitalla T, Zus F, Grzeschik M. 2011b.. Operational assimilation of GPS slant path delay measurements into the MM5 4DVAR system. *Tellus* **63A**: 263–282.

Behrendt A, Pal S, Aoshima F, Bender M, Blyth A, Corsmeier U, Cuesta J, Dick G, Dorninger M, Flamant C, Di Girolamo P, Gorgas T, Huang Y, Kalthoff N, Khodayar S, Mannstein H, Träumner K, Wieser A, Wulfmeyer V. 2011. Observation of convection initiation processes with a suite of state-of-the-art research instruments during COPS IOP8b. *Q. J. R. Meteorol. Soc.* **137**: 287–305.

Bénard P. 2004. 'ALADIN/AROME dynamical core, status and possible extension to IFS'. In *Proceedings of seminar on recent developments in numerical methods for atmospheric and ocean modelling, 6–10 September 2004*. ECMWF: Reading, UK.

Berre L, Stefanescu S, Belo Pereira M. 2006. The representation of the analysis in three error simulation techniques. *Tellus* **58A**: 196–209.

Bhawar R, Di Girolamo P, Summa D, Flamant C, Althausen D, Behrendt A, Kiemle C, Bosser P, Cacciani M, Champollion C, Di Iorio T, Engelmann R, Herold C, Pal S, Wirth M, Wulfmeyer V. 2011. The water vapour intercomparison effort in the framework of the convective and orographically-induced precipitation study: Airborne-to-ground-based and airborne-to-airborne lidar systems. *Q. J. R. Meteorol. Soc.* **137**: 325–348.

Bock O, Nuret M. 2009. Verification of NWP model analyses and radiosonde humidity data with GPS precipitable water vapor estimates during AMMA. *Weather and Forecasting* **24**: 1085–1101.

 

Boniface K, Ducrocq V, Jaubert G, Yan X, Brousseau P, Masson F, Champollion C, Chéry J, Doerflinger E. 2009. Impact of high-resolution data assimilation of GPS zenith delay on Mediterranean heavy rainfall forecasting. *Ann. Geophys.* **27**: 2739–2753.

Bougeault P, Binder P, Buzzi A, Dirks R, Houze R, Kuettner J, Smith RB, Steinacker R, Volkert H. 2001. The MAP special observing period. *Bull. Am. Meteorol. Soc.* **82**: 433–462.

Brousseau P, Berre L, Bouttier F, Desroziers G. 2011a. Background-error covariances for a convective-scale data-assimilation system: AROME-France 3D-Var. *Q. J. R. Meteorol. Soc.* **137**: 409–422.

Brousseau P, Berre L, Bouttier F, Desroziers G. 2011b. Flow-dependent background-error covariances for a convective-scale data assimilation system. *Q. J. R. Meteorol. Soc.* DOI: 10.1002/qj.920.

Browning KA, Morcrette CJ, Nicol J, Blyth AM, Bennett LJ, Brooks BJ, Marsham J, Mobbs SD, Parker DJ, Perry F, Clark PA, Ballard SP, Dixon MA, Forbes RM, Lean HW, Li Z, Roberts NM, Corsmeier U, Barthlott C, Deny B, Kalthoff N, Khodayar S, Kohler M, Kottmeier C, Kraut S, Kunz M, Lenfant J, Wieser A, Agnew JL, Bamber D, McGregor J, Beswick KM, Gray MD, Norton E, Ricketts HMA, Russell A, Vaughan G, Webb AR, Bitter M, Feuerle T, Hankers R, Schulz H, Bozier KE, Collier CG, Davies F, Gaffard C, Hewison TJ, Ladd DN, Slack EC, Waight J, Ramatschi M, Wareing DP, Watson RJ 2007. The convection storm initiation project. *Bull. Am. Meteorol. Soc.* **88**: 1939–1955.

Bruneau D, Quaglia P, Flamant C, J P. 2001a.. The airborne lidar LEANDRE II for water-vapor profiling in the troposphere. II. First results. *Appl. Opt.* **40**: 3462–3475.

Bruneau D, Quaglia P, Flamant C, Meissonnier M, J P. 2001b. The airborne lidar LEANDRE II for water-vapor profiling in the troposphere. I. System description. *Appl. Opt.* **40**: 3450–3461.

Bubnovà R, Hello G, Bénard P, Geylin J. 1995. Integration of the fully elastic equations cast in the hydrostatic pressure terrain-following coordinate in the framework of the ARPEGE/ALADIN NWP system. *Mon. Weather Rev.* **123**: 515–535.

Courtier P, Thépaut J, Hollingworth A. 1994. A stategy for operational implementation of 4D-VAR using an incremental approach. *Q. J. R. Meteorol. Soc.* **120**: 1367–1387.

Cuxart J, Bougeault P, Redelsperger JL. 2000. A turbulence scheme allowing for mesoscale and large-eddy simulations. *Q. J. R. Meteorol. Soc.* **126**: 1–30.

Dorninger M, Schneider S, Steinacker R. 2008. On the interpolation of precipitation over complex terrain. *Meteorol. Atmos. Phys.* **101**: 175–189, DOI:10.1007/s00703–008–0287–6.

Ducrocq V, Ricard D, Lafore JP, Orain F. 2002. Storm-scale numerical rainfall prediction for five precipitating events over France: On the importance of the initial humidity field. *Weather and Forecasting* **17**: 1236–1256.

Fischer C, Montmerle T, Berre L, Auger L, Stefanescu S. 2005. An overview of the variational assimilation in the ALADIN/FRANCE NWP system. *Q. J. R. Meteorol. Soc.* **131**: 3477–3492.

Grzeschik M, Bauer H, Wulfmeyer V, Engelbart D, Wandinger U, Mattis I, Althausen D, Engelmann R, Tesche M, Riede A. 2008. Four-dimensional variational data analysis of water vapor Raman lidar data and their impact on mesocale forecasts. *J. Atmos. Ocean. Technol.* **25**: 1437–1453.

Harnisch F, Weismann M, Cardinali C, Wirth M. 2011. Assimilation of DIAL water vapour observations in the ECMWF global model. *Q. J. R. Meteorol. Soc.* **137**: 1532–1546.

Kalthoff N, Adler B, Barthlott C, Corsmeier U, Mobbs S, Crewell S, Träumer K, Kottmeier C, Wieser A, Smith V, Di Girolamo P. 2009. The impact of convergence zones on the initiation of deep convection: A case study from COPS. *Atmos. Res.* **93**: 680–694.

Kamineni R, Krishnamurti T, Ferrare R, Ismail S, Browell EV. 2003. Impact of high resolution water vapor cross-sectional data on hurricane forecasting. *Geophys. Res. Lett.* **30**, 1234, DOI: 10.1029/2002GL016741.

Kamineni R, Krishnamurti T, Patinaik S, Browell E, Ismail S, Ferrare R. 2006. Impact of CAMEX-4 datasets for hurricane forecasts using a global model. *J. Atmos. Sci.* **63**: 151–174.

Kiemle C, Wirth M, Fix A, Rahm S, Corsmeier U, Di Girolamo P. 2011. Latent heat flux measurements over complex terrain by airborne water vapour and wind lidars. *Q. J. R. Meteorol. Soc.* **137**: 190–203.

Kottmeier C, Kalthoff N, Barthlott C, Corsmeier U, van Baelen J, Behrendt A, Behrendt R, Blyth A, Coulter R, Crewell S, Di Girolamo P, Dorninger M, Flamant C, Foken T, Hagen M, Hauck C, Höller H, Konow H, Kunz M, Mahlke H, Mobbs S, Richard E, Steinacker R, Weckwerth T, Wieser A, Wulfmeyer V. 2008. Mechanisms initiating deep convection over complex terrain during COPS. *Meteorol. Z.* **17**: 931–948.

Lafore JP, Stein J, Asencio N, Bougeault P, Ducrocq V, Duron J, Fischer C, Héreil P, Mascart P, Masson V, Pinty JP, Redelsperger JL, Richard E, Vilà-Guerau de Arellano J. 1998. The Meso–NH Atmospheric Simulation System. Part I: adiabatic formulation and control simulations. Scientific objectives and experimental design. *Ann. Geophys.* **16**: 90–109.

Masson V. 2000. A physically based scheme for the urban energy budget in atmospheric models. *Boundary-Layer. Meteorol.* **1994**: 357–397.

Mlawer EJ, Taubman SJ, Brown PD, Iacono MJ, Clough SA. 1997. Radiative transfer for inhomogeneous atmospheres: RRTM, a validated corrolated-*k* model for the longwave. *J. Geophys. Res.* **102D**: 16663–16682.

Montmerle T, Rabier F, Fischer C. 2007. Respective impact of polar orbiting and geostationary satellite observations in the ALADIN/FRANCE NWP system. *Q. J. R. Meteorol. Soc.* **133**: 655–671.

Noilhan J, Mafhouf J. 1996. The ISBA land surface parameterisation. *Global Planet Change* **13**: 145–159.

Nuret M, Lafore JP, Bock O, Guichard F, Agusti-Panareda A, Ngamini JB, Redelsperger JL. 2008. Correction of humidity bias for Vaïsala RS80 sondes during AMMA 2006 observing period. *J. Atmos. Ocean. Technol.* **25**: 2152–2158.

Pinty JP, Jabouille P. 1998. 'A mixed-phase cloud parameterization for use in a mesoscale non-hydrostatic model: simulations of a squall line and of orographic precipitations'. In *Conf. on Cloud Physics, Everett, WA, USA*. Amer. Meteorol. Soc.: Boston, MA; pp 217–220.

Redelsperger JL, Thorncroft C, Diedhiou A, Lebel T, Parker D, Polcher J. 2006. African Monsoon, Multidiscplinary Analysis (AMMA): An international research project and field campaign. *Bull. Am. Meteorol. Soc.* **87**: 1739–1746.

Richard E, Chaboureau JP, Flamant C, Champollion C, Hagen M, Schmidt K, Kiemle C, Corsmeier U, Barthlott C, Di Girolamo P. 2011. Forecasting summer convection over the Black Forest: a case study from the COPS experiment. *Q. J. R. Meteorol. Soc.* **137**: 101–117.

Rotach M, Ambrosetti P, Ament F, Appenzeller C, Arpagaus M, Bauer HS, Bouttier F, Buzzi A, Corazza M, Davolio S, Denhard M, Dorninger M, Fontannaz L, Frick J, Fundel F, Germann U, Gorgas T, Hegg C, Hering A, Keil C, Liniger M, Marsigli C, McTaggart-Cowan R, Montani A, Mylne K, Ranzi R, Richard E, Rossa A, Santos-Muoz D, Schär C, Seity Y, Staudinger M, Stoll M, Volkert H, Walser A, Wang Y, Werhahn J, Wulfmeyer V, Zappa M. 2009. MAP D-PHASE: Real-time demonstration of weather forecast quality in the Alpine region. *Bull. Am. Meteorol. Soc.* **90**: 1321–1336.

Seity Y, Brousseau P, Malardel S, Hello G, Bénard P, Bouttier F, Lac C, Masson V. 2011. The AROME-France convective scale operational model. *Mon. Weather Rev.* **139**: 976–991.

Steinacker R, Haberli C, Pottschacher W. 2000. A transparent method for the analysis and quality evaluation of irregularly distributed and noisy observational data. *Mon. Weather Rev.* **128**: 2303–2316.

Steinacker R, Ratheiser M, Bica B, Chimani B, Dorminger M, Grepp W, Lotteraner C, Schneider S, Tschannett S. 2006. A mesoscale data analysis and downscaling method over complex terrain. *Mon. Weather Rev.* **134**: 2758–2771.

Weckwerth T, Parsons DB, Koch SE, Moore JA, LeMone MA, Demoz BB, Flamant C, Geerts B, Wang J, FeltzWF. 2004. An overview of the International H2O Project (IHOP-2002) and some preliminary highlight. *Bull. Am. Meteorol. Soc.* **85**: 253–277.

Wirth M, Fix A, Schwarzer H, Schrandt F, Ehret G. 2009. The airborne multi-wavelength water vapor differential absorption lidar WALES: system design and performance. *Appl. Phys.* **96**: 201–213, DOI:10.1007/s00340–009–3365–7.

Wulfmeyer V, Bauer H, Grzeschik M, Behrendt A, Browell E, Ismai S, Ferrare R. 2006. Four-dimensional variational assimilation of water vapor differential absorption lidar data: The first case study within IHOP-2002. *Mon. Weather Rev.* **134**: 209–230.

Wulfmeyer V, Behrendt A, Bauer HS, Kottmeier C, Corsmeier U, Blyth A, Craig G, Schumann U, Hagen M, Crewell S, Di Girolamo P, Flamant C, Miller M, Montani A, Mobbs S, Richard E, Rotach M, Arpagaus M, Russchenberg H, Schlüssel P, König M, Gärtner V, Steinacker R, Dorninger M, Turner D, Weckwerth T, Hense A, Simmer C. 2008. The convective and orographically-induced precipitation study (COP): A research project for improving quantitative precipitation forecasting in low-mountain regions. *Bull. Am. Meteorol. Soc.* **89**: 1477–1486.

Wulfmeyer V, Behrendt A, Kottmeier C, Corsmeier U, Barthlott C, Craig G, Hagen M, Althausen D, Aoshima F, Arpagaus M, Bauer HS, van Baelen J, Bennett L, Blyth A, Brandau C, Champollion C, Crewell S, Dick G, Dorninger M, Dufournet Y, Eigenmann R, Engelmann R, Flamant C, Foken T, Di Girolamo P, Groenemeijer P, Gorgas T, Grzeschik M, Peters G, Handwerker J, Hauck C, Höller H,

 

Junkermann W, Kalthoff N, Kiemle C, König M, Krauss L, Long C, Madonna F, Mobbs S, Neininger B, Pal S, Pigeon G, Richard E, Rotach MW, Russchenberg H, Schwitalla T, Smith V, Steinacker R, Trentmann J, Turner DD, Vogt S, Volkert H, Weckwerth T, Wernli H, Wieser A. 2011. The Convective and Orographically-induced Precipitation Study (COPS): The scientific strategy, the field phase, and first highlights. *Q. J. R. Meteorol. Soc.* **137**: 3–30.

Yan X, Ducrocq V, Jaubert G, Brousseau P, Poli P, Champollion C, Flamant C, Boniface K. 2009. The benefit of GPS zenith delay assimilation to high-resolution quantitative precipitation forecasts: A case-study from COPS IOP 9. *Q. J. R. Meteorol. Soc.* **135**: 1788–1800.

Zus F, Grzeschik M, Bauer HS, Wulfmeyer V, Dick G, Bender M. 2008. Development and optimization of the IPM MM5 GPS slant path 4DVAR system. *Meteorol. Z.* **17**: 867–885.

 